Simulation Technique for Pre-forming of AHSS Edge Stretching

Xiaoming Chen*, Jixin Sun** and Xinhai Zhu**
** United States Steel Automotive Center, 5850 New King Court, Troy, MI, USA*
*** Livermore Software Technology Corp., Livermore, CA, USA*

Abstract

Edge cracking in advanced high strength steels (AHSS) is one of the main failure modes in many sheet metal stamping processes. Pre-forming into a wave (or scallop) shape at the edge is a common technique used to gain material at high edge stretch regions in preparation for the subsequent edge stretch processes. The accurate simulation of this multi-stage forming process remains a challenging task since these edges experience complicated forming processes including bending, unbending, and stretching deformations. In this study, a simulation variable study is performed and the effect of various material models, hardening rules and solvers on the simulation results is also investigated. A simulation technique is established for this multi-stage forming process. Simulation results are compared to experimental data and reasonable agreement is achieved. Different failure criteria are also evaluated and discussed for use in this type of application.

Introduction

Bending and un-bending are common deformation modes in sheet metal forming processes. For example, forming processes such as drawing over a die radius, passing through drawbeads, and pre-forming a sheet edge then flanging involve bending/un-bending deformation. The computer simulation technology for those processes is well established for conventional sheet steels. However, this simulation technology is not always applicable to AHSS forming processes since AHSS show significantly different material microstructures from the conventional mild or high-strength steels. Therefore, the direct application of the simulation methods used for the conventional steels to AHSS may result in inaccurate predictions of some of the manufacturing issues in AHSS stamping such as edge cracking, stretch-bending fracture in a tight radius (shear fracture), and springback. Due to the high-strength and multi-phase microstructure of AHSS, the edge cracking and shear fracture limits of AHSS are significantly lower than those of the conventional steels. Unlike the conventional steels, those limits for AHSS cannot be predicted using the conventional forming limit curve (FLC), as shown in Figure 1 for shear fracture and in Figure 2 for edge cracking with pre-forming. In both cases, the FLC failed to predict shear fracture in the radius and edge cracking at edges. The presence of significant Bauschinger effects plus the higher strength in AHSS requires new simulation technology to predict springback, since the conventional simulation method usually shows under-prediction. Due to those challenges in computer simulations, the stamping tool and process designs for AHSS often involve significant trial and error procedures. Therefore, the accurate prediction of those manufacturing issues using computer simulations is necessary to shorten the lead time and to reduce the cost of tool and die development processes. In the last several years, significant research has been conducted to improve the accuracy of computer simulations to solve those AHSS manufacturing issues.

In the study of edge cracking of AHSS, the hole expansion and tension tests are usually used. Several experiments [1-3] were conducted to investigate the effects of different shearing methods, process parameters, and sheared edge characters on AHSS edge cracking. The pre-

forming effect was also investigated in a recent study [4]. Various simulation techniques were used to integrate the deformation during shearing into hole expansion analyses to provide more accurate results. Different failure criteria were also used to improve the AHSS edge cracking predictability [5, 6]. In the study of AHSS shear fracture, various experiments [7, 8] were conducted to duplicate the failures at different stretch bending radii and in different stretching levels during bending and an empirical shear fracture limit was proposed for various AHSS. Alternative failure criteria were also used in simulations to improve the fracture predictions [9]. In springback studies, the prediction accuracy was significantly improved by using the kinematic/isotropic hardening material models for AHSS and other simulation technologies [10, 11].

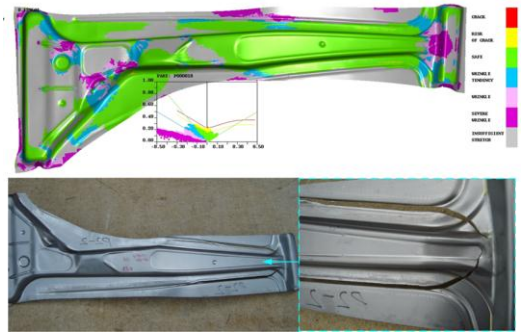

Figure 1. Shear fracture at drawbeads.

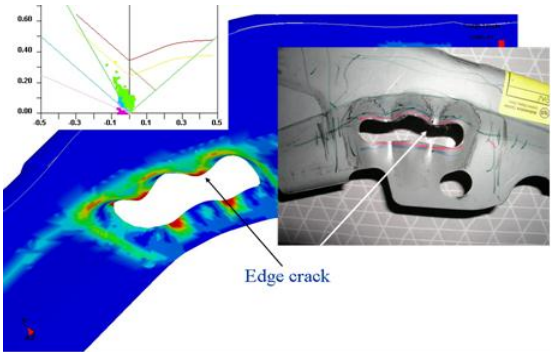

Figure 2. AHSS edge crack with pre-forming.

In flanging or edge stretching of the conventional steels, the edge is usually formed into a wave (or scallop) shape in a previous stage for gaining material in the final stretching stage. However, this technique is not applicable to AHSS stamping in many cases. Figure 2 shows an example of pre-forming, trimming, and then flanging processes of dual phase (DP) 780 steel, a common procedure employed in forming the conventional mild steels. In this case, cracks occur at the edges in the pre-forming stage and the part cannot withstand flanging in the next stage. This complicated pre-forming and stretch forming process involves bending, unbending, and edge stretching deformations, which may result in the three AHSS issues discussed above. Little work has been done on the history and evolution of the sheet surface strains during pre-forming. In this work, simulation studies and experimental correlations were conducted on pre-forming and subsequent edge stretching for two AHSS steels (DP780 and 590R). The digital image correlation (DIC) technique was used to measure the deformation and surface strain history during both pre-forming and subsequent stretching. The finite element analysis was also conducted to simulate those processes using LS-DYNA® software package. A systematic simulation study was conducted involving various simulation variables including three yield criteria (von Mises, Hill's 1948 and Barlat), isotropic and isotropic/kinematic hardening rules, implicit and explicit solvers.

Experiment Summary

To better understand the pre-forming effect, experiments were designed to duplicate pre-forming and stretching in the laboratory for DP780 and 590R. The mechanical properties for tested materials are shown in Table 1. The experimental data generated in the experiment were used for the validation of the simulation techniques used in the simulations.

Table 1. Mechanical Properties

Material	Yield Strength (MPa)	UTS (MPa)	Total Elong (%)	n value	r average
590R	440	636	22.9	0.134	0.77
DP780	497	856	15.0	0.122	0.84

Tests for Pre-forming and Stretching

The bending/unbending deformation in a pre-forming process can be experimentally created by the tool shown in Figure 3. Using this tool, a pre-formed wave can be created from a straight steel strip. Both one and two waves can be made with three different radii and various pre-form depths. Figure 4 shows some of those pre-formed specimens.

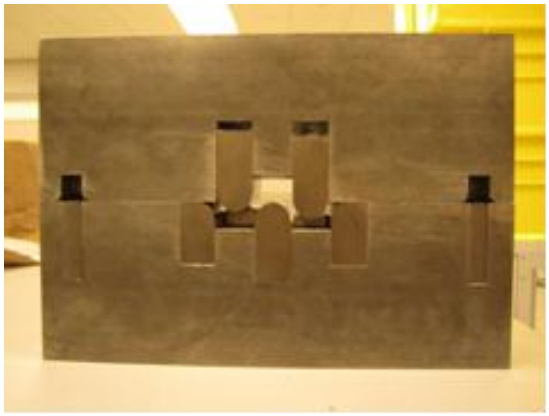

Figure 3. Tools for pre-forming.

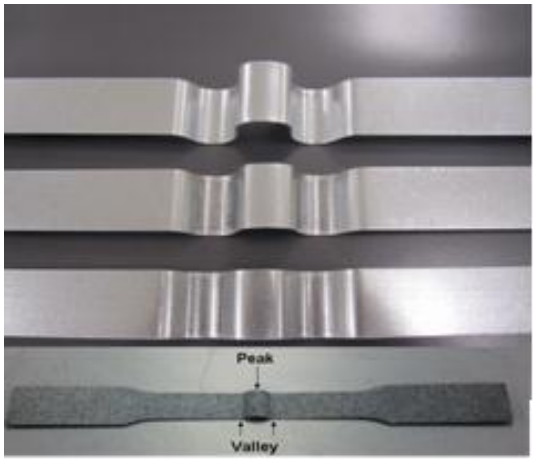

Figure 4. Pre-formed strip.

Since edge stretching is in a uniaxial tension state, its deformation can be experimentally simulated by a tensile test. Therefore, subsequent stretching of the edges can be simulated by pulling a pre-formed strip in a tension test. The tension test with a DIC system for strain measurement is shown in Figure 5. The full field strain distribution and strain history can be captured by the DIC system.

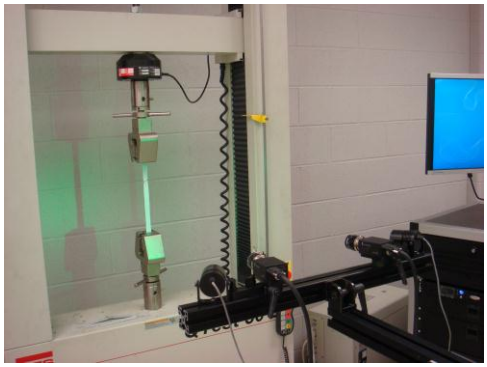

Figure 5. Stretching of pre-formed strip.

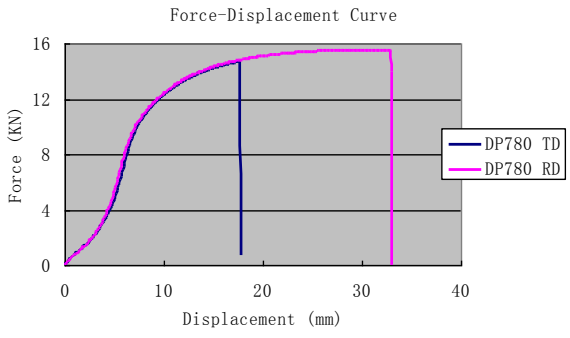

Figure 6. Force-displacement curves.

Strain Distributions

Figure 7 shows the color maps of true major and minor strain distributions on the top surface of a pre-formed sample. The maximum strain is about 7% at the peak of the pre-formed strip. Figures 8 and 9 show the strain distributions at fracture in the tension test for DP780 and 590R, respectively. As shown in the figures, the DIC technique can obtain the strain distributions clearly and capture the strains at fracture.

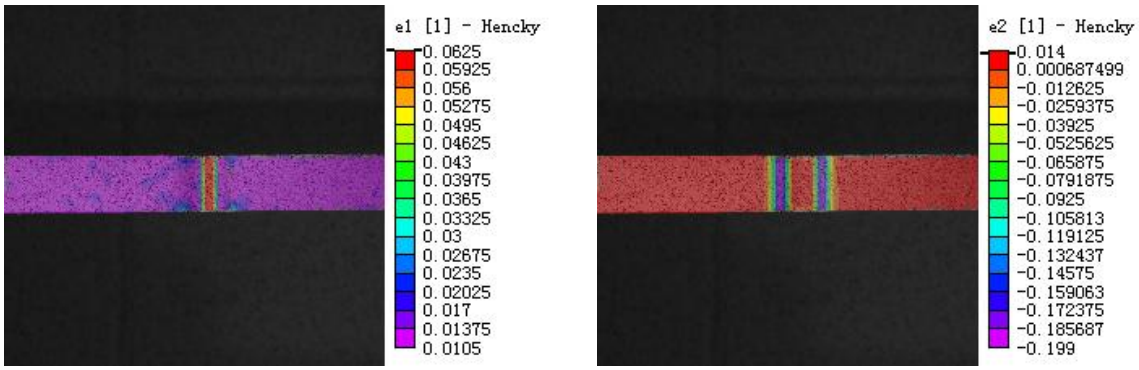

(a) (b)

Figure 7. Major (a) and minor (b) strain distributions on a pre-formed sample of DP780.

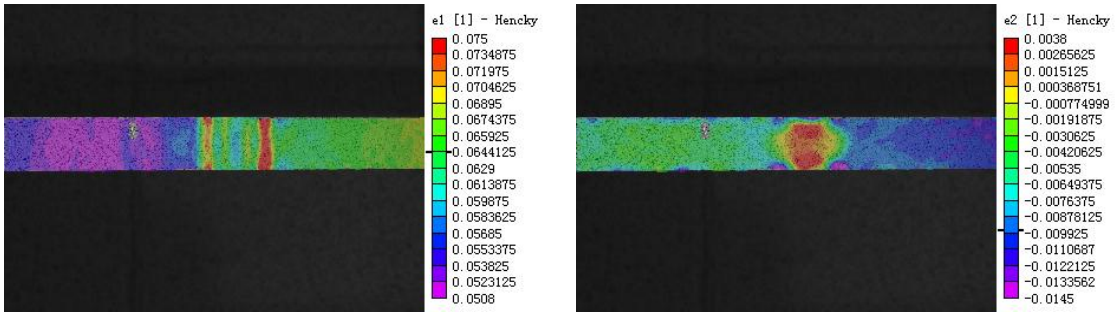

(a) (b)

Figure 8. Major (a) and minor (b) strain distributions at fracture (DP780 transverse).

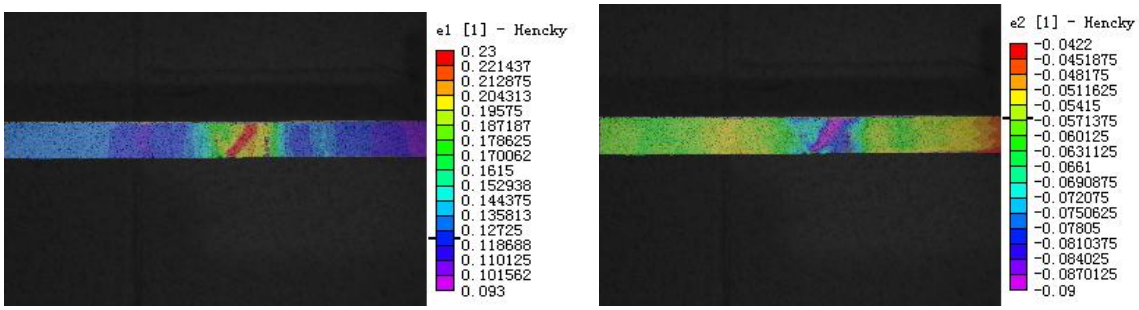

(a) (b)

Figure 9. Major (a) and minor (b) strain distributions at fracture (590R transverse).

The deformation history recorded by the DIC system provided very useful information for multi-stage forming analyses as in the current case. The above strain mapping figures show that the major and minor strain distributions are reasonably uniform along the width of the specimens. Therefore, the deformation history can be evaluated using one section along the width. Using

one section data along the width, the major strains measured on the top surfaces at various steps are shown in Figures 10 to 13. During the first step forming (pre-forming), bending is the dominant deformation, in which tension is at the peak and compression at the valleys. During the subsequent stretching in the tension machine, unbending is occurring at the pre-formed region as the specimen is stretching and tension strain is increasing along the whole specimen.

For the specimens cut in the transverse direction (bending and specimen width in the rolling direction), fracture occurs in the pre-formed regions as shown in Figures 10 and 11 for DP780 and 590R steels, respectively. For the specimens cut in the longitudinal direction, fracture occurs outside the pre-formed regions and the fracture strain is significantly higher than those from the transverse cut specimens, as shown in Figures 12 and 13 for DP780 and 590R steels, respectively.

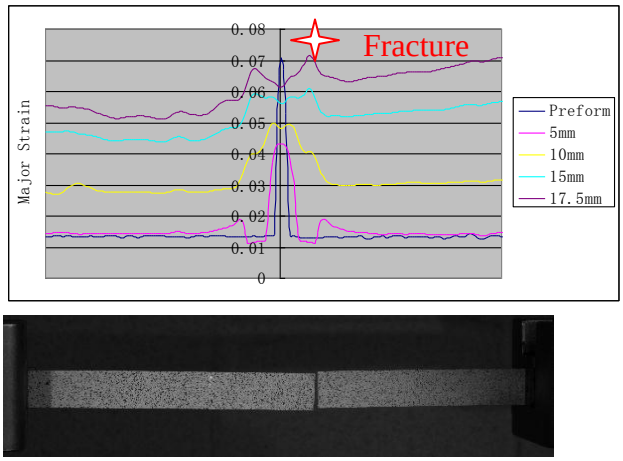

Figure 10. Major strain of DP780 along transverse direction.

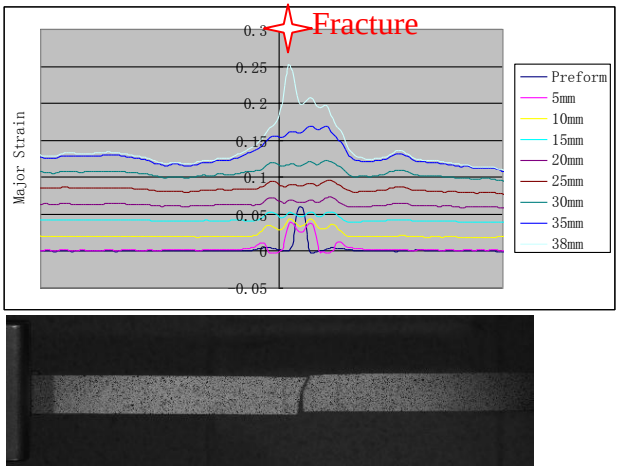

Figure 11. Major strain of 590R along transverse direction.

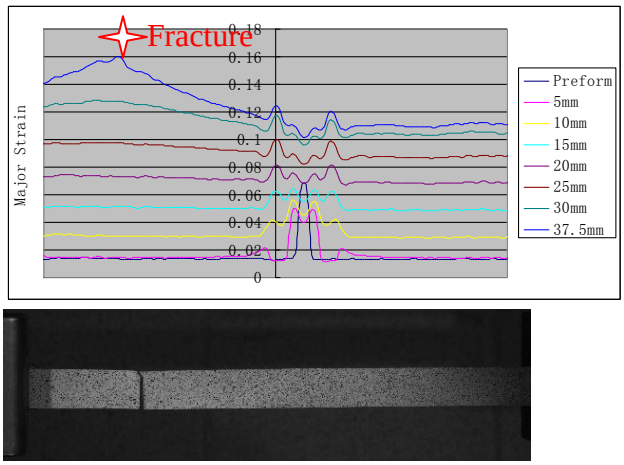

Figure 12. Major strain of DP780 in the rolling direction.

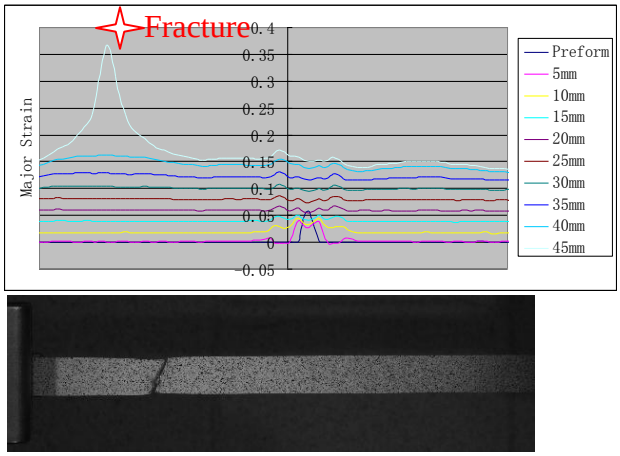

Figure 13. Major strain of 590R in the rolling direction.

Fracture

Three types of tensile failures were observed in the tension tests for DP780, as shown in Figure 14. Type A occurred when the specimen was milled from an as-received flat sheet and in this case the specimen had no pre-strain and no edge damage from shearing. Fracture initiated from the center of a specimen. Thinning and necking were also observed in the specimen. Type B occurred when the specimen was prepared from an as-received flat sheet using a typical die shearing process. In this case, the specimen had no pre-strain with edge damage from shearing and minor necking and thinning were observed around the fracture line. Type C occurred when a sheared edge specimen was pre-formed then pulled in the tension. In this case, the specimen was pre-formed with edge damage from shearing and fracture occurred at the pre-formed region and initiated at the edge with little thinning and necking. Figure 15 shows the comparison in the fracture strains for those three types of failures. There is a critical strain value for the pre-forming and stretching process. This critical strain value depends on the pre-forming geometry, edge damage severity, steel grade and material orientation. If this critical strain value is not reached, failure occurs at the outside of the pre-formed region.

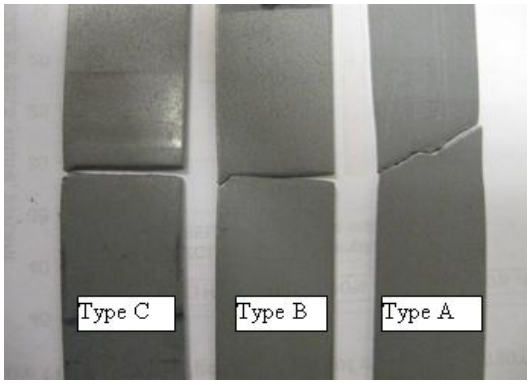

Figure 14. Three type of fractures of DP780steel.

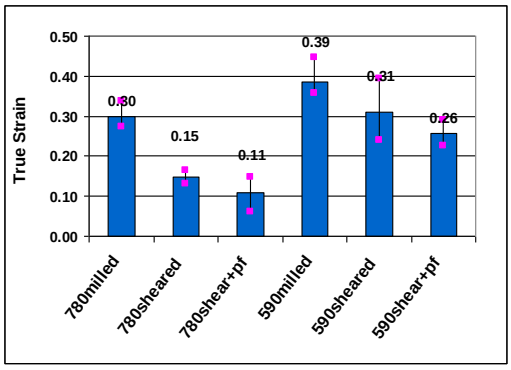

Figure 15. Comparison of the fracture strain for three types (A, B and C).

Simulation

FEA Model and Simulation Setup

Finite element analyses using LS-DYNA® software were conducted to simulate the pre-forming and stretching tests. Only half of the blank width was used due to the symmetry of the sample, as shown in Figure 16. Both full integration shell elements and solid elements were used in this study. The results from an initial simulation using a typical simulation setup for a forming simulation process did not agree well with the testing data. Therefore, a sensitivity study was then conducted on various simulation variable setups including three yield criteria (von Mises, Hill's 1948 and Barlat), isotropic and isotropic/kinematic hardening rules, implicit and explicit solvers. Strain distribution is usually used to evaluate a forming process. Therefore, the strain distribution along the specimen length (Exx) at different strain histories is used to evaluate the sensitivity of various simulation variables on the simulation results.

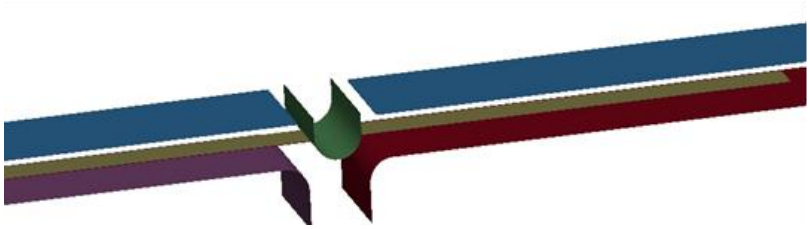

Figure 16. Finite element model for simulation

Variable Study and Results Comparison

There was no significant difference in the simulation results for those three yield criteria used in the simulation. Therefore, Hill's yield criterion was selected in all other simulations since it gave a slightly better result.

Figure 17 shows the Exx distribution during pre-forming using various combinations of simulation variables. It is seen that there is no significant difference among the various simulation setups. Figure 18 shows the Exx distribution history during pre-forming and subsequent stretching using the isotropic hardening material model and explicit solver. The X axis is the location along the length of specimen and the Y axis is the Exx distribution at different time steps. The first line from the bottom is the Exx distribution after pre-forming and 2nd to 4th lines from the bottom are Exx distributions corresponding to 3%, 6%, 9% and 12% stretch levels, respectively, in the subsequent stretching testing. It is observed that as the specimen is stretching after pre-forming, unbending occurs at the pre-formed region and the tension strain is increasing across the entire length of the specimen. However, in the pre-form region, the maximum Exx stops increasing when it reaches 0.08, even when tensile stretching continues. Deformations distribute to other regions. This maximum strain (0.08) is lower than the fracture strain measured in the experiment. Therefore, this simulation setup could not predict the correct strain distribution and fracture in this case. The Exx distribution history during pre-forming and subsequent stretching is shown in Figure 19 using the isotropic hardening material model and implicit solver and in Figure 20 using the isotropic/kinematic hardening material model and explicit solver. Similarly these two combinations also under-predict the strains in the pre-formed region.

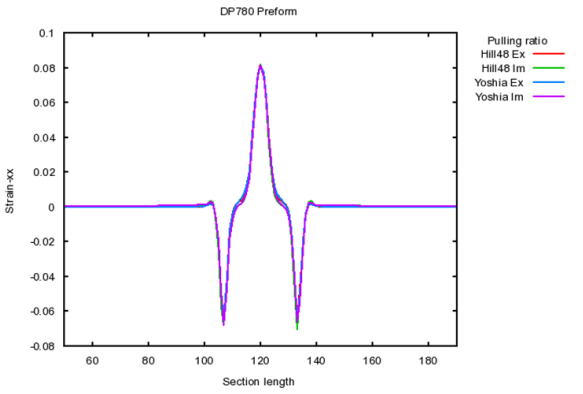

Figure 17. Exx of pre-forming for various simulation combinations.

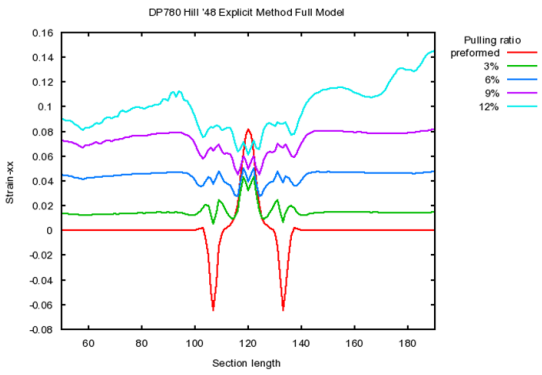

Figure 18. Exx history using isotropic hardening and explicit solver.

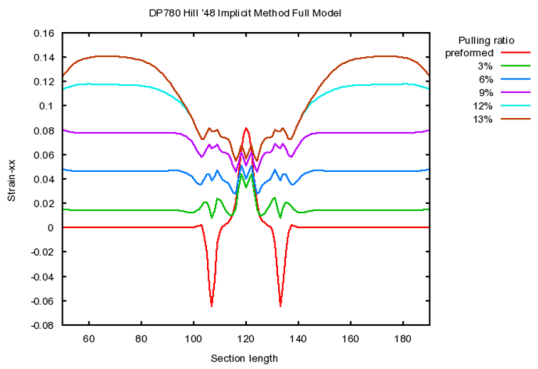

Figure 19. Exx history using isotropic hardening and implicit solver.

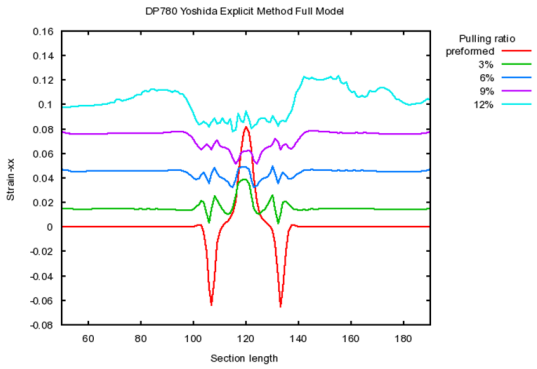

Figure 20. Exx history using kinematic hardening and explicit solver.

Figure 21 shows the Exx distribution history during pre-forming and subsequent stretching using the isotropic/kinematic hardening material model and implicit solver. It is seen that the strain distribution and strain levels in the pre-formed region at larger stretch levels are significantly different from those shown in Figures 18 to 20. Actually, this combination of simulation setup did predict the fracture strain in the pre-formed region as measured in the experiment. The presence of a significant Bauschinger effect causes the different deformation behaviors when AHSS steels are subjected to cyclic loading process. The kinematic hardening law needs to be used to model the AHSS hardening in loading and reverse loading conditions. When using the implicit solver for this analysis, the selection of an incremental time step is very important. Time steps that were too small induce a high cost in computational time. Time steps that were too large may cause the computation to miss some critical deformation points, which would under-predict the bending/unbending strains. The comparison in the Exx distribution at different deformation levels between the simulation and experimental results are shown in Figure 22 for DP780 and in Figure 23 for 590R. It is seen that the predicted results agree reasonably well with the experimental data for both materials. Therefore, the isotropic/kinematic hardening material model and implicit solver are recommended for this multi-stage forming process.

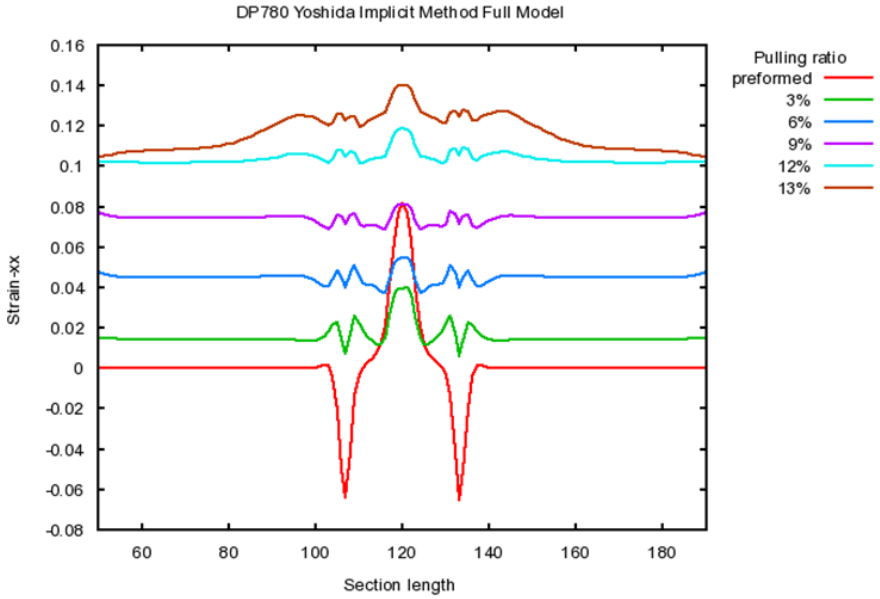

Figure 21. Exx history using isotropic/kinematic hardening and implicit solver.

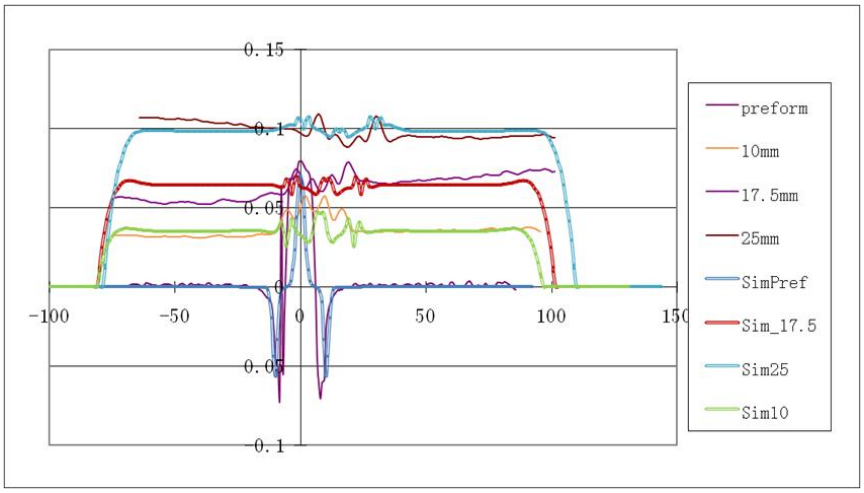

Figure 22. Exx comparison of simulation with experimental result for DP780.

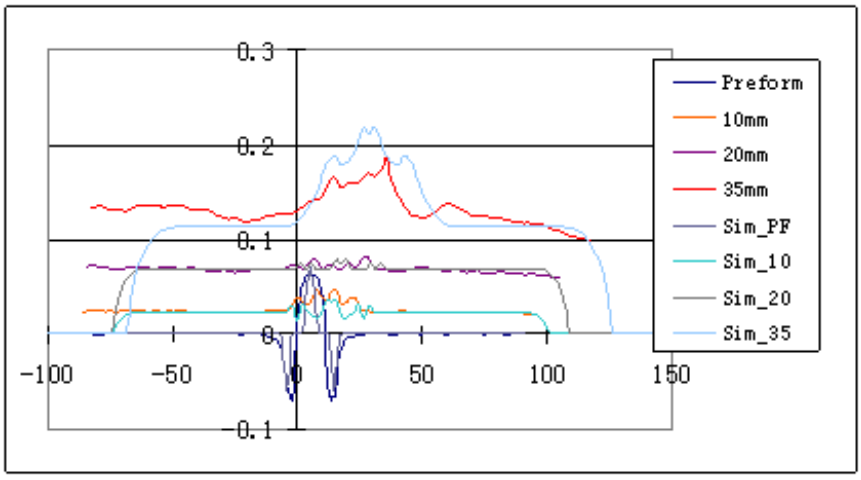

Figure 23. Exx comparison of simulation with experimental result for 590R.

The Forming Limit

The strain distribution at the edge when fracture is initiated is displayed in the forming limit diagram (FLD), as shown in Figure 24. All strain points at the edge are along the uniaxial tension line and are far below the conventional forming limit curve (FLC) for this material. This indicates that the conventional FLC cannot be used to predict AHSS edge cracking.

During pre-forming and subsequent stretching for the specimen used in the experiment, the strain path is different at various locations and therefore, their corresponding limit strains are not the same. Figure 25 shows possible limit strains at four different locations with different strain paths. The edge peak strain (EP) in the pre-formed region follows along the uniaxial tension path during bending and unbending and subsequent stretching. The edge valley point (EV) in the pre-formed region follows along the uniaxial compression strain path. The center peak point (CP) in the pre-formed region is in plane strain condition and follows along the major strain axis strain

path. The center valley point (CV) follows along the minor strain axis path. All horizontal lines represent the failure or limit strain measured in the experiment (major strain): 0.3 for the milled edge specimen, 0.15 for the sheared edge specimen and 0.11 for the sheared edge with pre-forming.

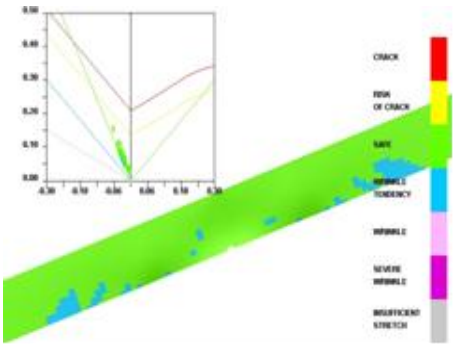

Figure 24. FLD strain mapping at fracture initiation.

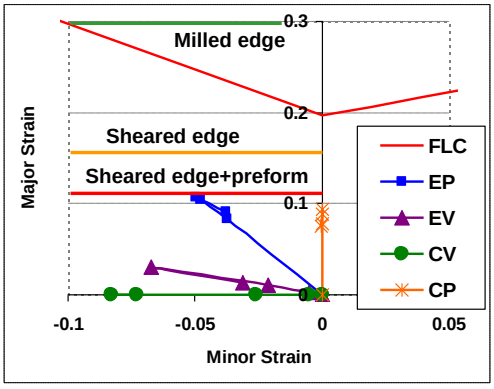

Figure 25. Comparison of different forming limits and strain paths.

Discussions

Implicit method vs. explicit method

As shown above, the results obtained using the implicit method are different from those using the explicit method. Unlike the implicit method, the explicit method failed to predict the correct peak strain in the pre-formed region. In general, the explicit method is more suitable for the transit problems, but for a quasi-static problem like the test in this study, more errors are expected. Those errors may be minimized by: a) decreasing the time step and b) reducing loading speed. In both cases, more explicit steps have to be used. The implicit method is more suitable for a quasi-static problem. In the implicit method, as long as the convergence tolerance is small enough, the force balance is reached for each step. This computation process is validated in the current case. This study also showed that the strain level in the center of the sample continues to increase during the stretching phase, a phenomenon observed from the test. Accordingly, the implicit method is recommended for the current study, which is a quasi-static problem.

Implicit time step

During the implicit calculation, the time step plays an important role in the final results, and it is found that very small time steps have to be used to avoid computation errors. In a typical stretching case, the material's flow stress increases as stretch increases due to the material strain hardening while, at the same time, the material thickness decreases. Higher flow stress due to strain hardening increases the resultant force while material thinning reduces the resultant force. At the early stage, the resultant force increases due to the high strain hardening rate and the lower rate of material thinning. However, after a certain strain level, the process reverses and the overall resultant force decreases, as shown in Figure 26. In the implicit calculation of current

model, all the elements are very regular and small. A large time step can easily miss the maximum resultant force point and the deformation can go from a very low point to a point bypassing the peak force, which would result in a wrong solution. For this reason, a small time step was used in this study to ensure the peak point is not missed in the simulation.

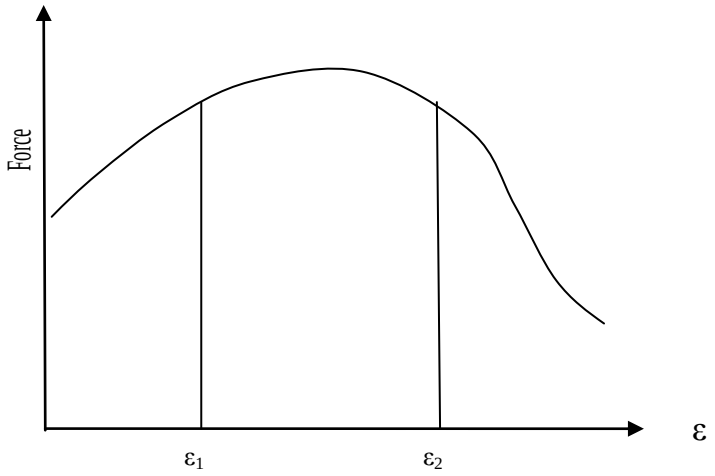

Figure 26. Illustration of force vs. strain effective strain during stretching.

Conclusions

The following conclusions can be made from this study:

- Pre-forming is an important forming process in the prevention of edge cracking in flanging and edge stretching processes. The conventional approach needs to be modified for use in AHSS pre-forming and for the simulation technique.
- Surface strain distributions during pre-forming and subsequent stretching can be measured with the DIC technique, which provides a full field and a history of strain distributions.
- There is a critical strain value during pre-forming and subsequent edge stretching, which determines if the failure location is in or out of the pre-formed region. This strain value depends on the pre-formed geometry, edge damage severity, steel grade, and material orientation.
- The conventional FLC cannot be used to predict edge failure in pre-forming and subsequent stretching since the failure or limit strain in this case is much lower than the limit strain determined based on the localized neck due to the sheared edge damage and stretch bending deterioration. The limit strain can be measured with the pre-forming and stretch testing.
- Simulation technologies have been established to accurately predict the strains during pre-forming and subsequent stretching. This simulation technology uses an implicit solver with the isotropic/kinematic hardening material model. With this simulation technique, optimal designs of pre-forming including geometry/shape and severity of bending can be carried out for a given AHSS material.

Acknowledgments

The authors would like to acknowledge the Department of Energy for funding and Auto-Steel Partnership High Strength Steel Team for supporting this project.

REFERENCE

1. A. Konieczny and T. Henderson, "*On Formability Limitations in Stamping Involving Sheared Edge Stretching*," SAE technical paper 2007-01-0340.
2. A J. Chintamani and S. Sriram, "*Sheared Edge Characterization of Steel Products used for Closure Panel Applications*," SAE technical paper 2006-01-1589.
3. Jian Wang, Todd Link, Mattew Merwin, "*AHSS Edge Formability in Sheared Edge Tension*," International Conference on New Developments in Advanced High-Strength Sheet Steels, 2008.
4. Xiaoming Chen, Ke Chen, Lorenzo Smith, "Pre-Forming Effects on AHSS Edge Cracking ," Proc. of Numisheet 2011, Soul, Korea.
5. X. M. Chen, C.Du, X. Wu, X. Zhu and S-D. Liu, "*Sheet Metal Shearing and Edge Characterization of Dual Phase Sheets,"* IDDRG International Conference, June 2009.
6. M. F. Shi and X. Chen, "*Stretch Flange-ability Limits of Advanced High Strength Steels*," SAE technical paper 2007-01-1693.
7. Hua-Chu Shih and Ming F. Shi, *"Experimental Study on Shear Fracture of Advanced High Strength Steels*," MSEC-ICMP 2008-72046.
8. H. Kim, A. R. Bandar, Y. P. Yang, J. H. Sung, and R. H. Wagoner, "Failure Analysis of Advanced High Strength Steels (AHSS) During Draw Bending," International Deep Drawing Research Group, Golden, CO, USA, pp. 449-460, 2009.
9. Xiaoming Chen, Meng Luo, et.al, "*AHSS Shear Fracture Predictions Based on a Recently Developed Fracture Criterion,"* SAE technical paper, 2010-01-0988.
10. Ming F.Shi, Xinhai Zhu, Cedric Xia, Thomas Stoughton, "*Determination of Non-linear Isotropic/Kinematic Hardening Constitutive Parameters for AHSS using Tension and Compression Tests*," Numisheet 2008.
11. Xiaoming Chen, et. al, "*Springback Prediction Improvement Using New Simulation Technologies*," SAE technical paper 2009-01-9881.